Respiration-Induced Kidney Motion on Cobalt-Chromium Stent Fatigue Resistance

Hao-Ming Hsiao,[1] Alexander Nikanorov,[1] Santosh Prabhu,[1] Mahmood K. Razavi[2]

[1] Abbott Laboratories, Abbott Vascular, Santa Clara, California 95054

[2] St. Joseph Vascular Institute, Orange, California 92868

Received 15 July 2008; revised 23 January 2009; accepted 2 April 2009
Published online 8 June 2009 in Wiley InterScience (www.interscience.wiley.com). DOI: 10.1002/jbm.b.31424

Abstract: During normal breathing, the kidneys move up and down due to the diaphragm motion and the renal artery subsequently experiences bending at or close to its point of fixation to the aorta. The impact of this kidney motion on implanted stent fatigue performance was not well understood in the past. Previous study from the authors on an 18-mm long single cobalt-chromium stent showed that the change in bending angle was minor during simulated respiration-induced kidney motion on cadavers. Finite Element Analysis revealed excellent fatigue resistance of the studied cobalt-chromium stent under simulated respiratory motion for the single stent configuration. In this article, the study was extended further to the overlapped stent configuration where a physician deploys two stents overlapping at the stent ends to fully cover a long lesion. Fluoroscopic images showed that the change in bending angle during simulated respiration-induced kidney motion on cadavers was more significant when two cobalt-chromium stents were overlapped. Calculated data of the Goodman analysis for the overlapped stents migrated toward the Goodman diagram failure line, indicating lower fatigue resistance during respiration when compared to a single stent. © 2009 Wiley Periodicals, Inc. J Biomed Mater Res Part B: Appl Biomater 91B: 508–516, 2009

Keywords: cobalt-chromium stent; respiration; kidney; renal artery; fatigue; stent fracture

INTRODUCTION

Atherosclerotic renal artery stenosis is the most common disorder of the renal arterial circulation. Untreated renal artery stenosis can lead to progressive hypertension, renal insufficiency, kidney failure, and increased mortality. Despite the proven efficacy of traditional surgical procedures such as endarterectomy and renal artery bypass, endovascular therapy has emerged as an effective strategy for treatment. Renal angioplasty and endoluminal stenting are performed at an increasing rate, especially in patients with the most complex form of the disease.[1,2] Balloon-expandable stents for aorta-ostial renal artery stenosis is demonstrated to be a safe and effective therapy.[3] It offers more permanent relief to patients without lifelong prescription for medications or surgical procedure.

During normal breathing, the kidneys move up and down due to the diaphragm motion and the renal artery subsequently experiences bending at or close to its point of fixation to the aorta. Figure 1 shows the angiograms of the kidney and renal artery motion during respiration. It is unclear what impact this kidney motion has on stents implanted in renal arteries. This kidney/arterial motion is important in the evaluation of patients receiving cobalt-chromium stents in order to understand potential risks of stent fractures or in-stent restenosis associated with renal stenting. Although stent fractures in various vascular and nonvascular beds may not necessarily threaten the patient life, it is an undesirable event that should be avoided if possible. A literature review revealed that stent fractures have been observed in renal arteries. Bessias et al. reported stent thrombosis in a 47-year-old patient with a single kidney and diseased renal artery who underwent implant of a balloon-expandable stent.[4] The patient presented 25 days after the procedure with renal insufficiency and uncontrolled hypertension. Angiography showed a thrombosed stent that required an aortorenal bypass. The explanted renal artery revealed a fractured incompletely expanded stent. Similarly, Sahin et al. observed a fractured stent in a 55-year-old patient with mobile kidney.[5] They observed that fracture of the stent resulted from mobility of the left kidney, and suspected that the intimal hyperplasia the patient had 2 months after stenting might have been triggered by inflammatory reaction at the stent fracture points, due to destruction and irritation of the vessel wall. The former case report underscores the possibility of "missed"

Correspondence to: H.-M. Hsiao (e-mail: hao-ming.hsiao@av.abbott.com)
Contract grant sponsor: Abbott Laboratories, Abbott Vascular Division.

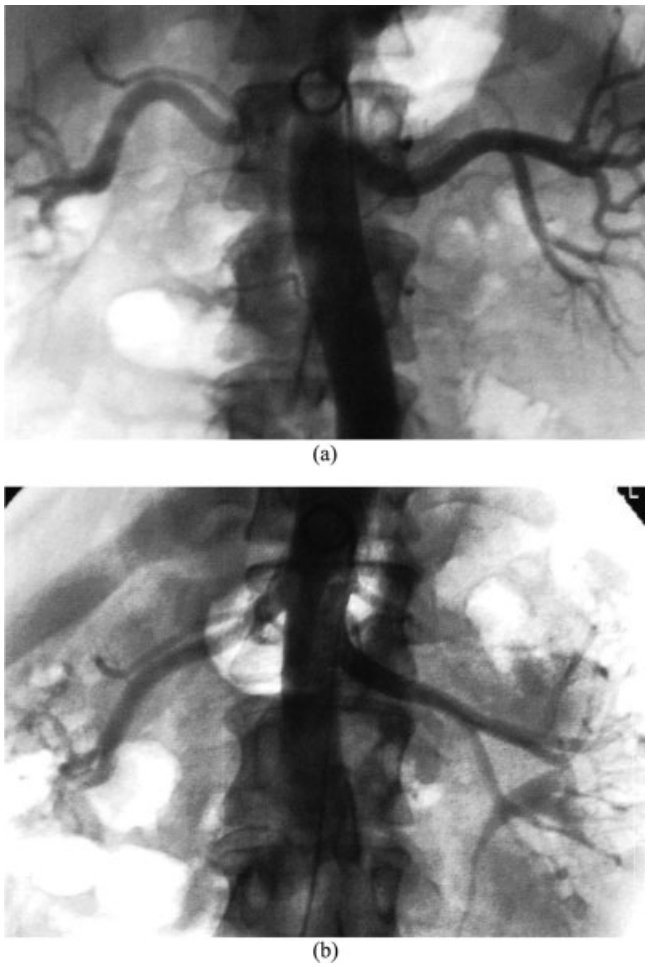

Figure 1. Angiographic images showing kidney and renal artery motion during respiration (a) Expiration, (b) Inspiration.

fractures in cobalt-chromium stents that could lead to restenosis and/or thrombosis, and the latter points to a possible mechanism. Stent fractures in renal arteries are difficult to identify and may be missed if they are not carefully looked for.

Earlier studies investigated the impact of respiration-induced motion of the kidneys for the purpose of radiotherapy planning to accurately treat tumor. These studies provide limited quantitative information on kidney movement.[6–9] In these studies, the kidneys moved ~20–40 mm in the craniocaudal dimension during normal respiration. Additionally, magnetic resonance imaging revealed that displacements of the left and right kidney during normal respiration varied from 2 to 24 mm and 4 to 35 mm, respectively.[6] Forced respiration (maximal inspiration and expiration) displacement of the left and right kidney varied from 10 to 66 mm and 10 to 86 mm, respectively. A recent study[10] evaluated not only kidney movement, but also the displacement and bending of the renal arteries during respiration using enhanced magnetic resonance angiography in healthy male volunteers. It was found that the renal ostia were relatively fixed, displacing a distance 10-fold less than that of the kidneys. The differential in displacement between the renal ostia and the kidneys resulted in statistically significant changes in renal branch angle. This raised the question of whether the motion of the kidneys and subsequent bending of the arteries would negatively impact cobalt-chromium stent fatigue performance and cause stent fractures. Stent fracture might trigger intimal hyperplasia that leads to restenosis.

In the current medical device industry, most of the coronary and endovascular stents are assessed using accelerated *in vitro* fatigue testing and Finite Element Analysis (FEA) to ascertain whether the device will survive a fatigue life of 10 years under simulated physiological loading conditions. To design against such fatigue failures, the majority of prior research on stent fatigue has focused on determining the stress/strain-life (*S-N*) properties of wires and stents.[11–13] Marrey et al. developed a new damage-tolerant analysis for quantitatively predicting the fatigue life of a cobalt-chromium stent.[14] Their approach was to base the primary fatigue-life assessment on a traditional, yet conservative version of an *S-N* analysis, and to further use fracture mechanics in order to evaluate the role of pre-existing flaws. Similar work has been extended to the nickel-titanium stents for endovascular applications.[15]

Hsiao et al. presented the first evaluation of the impact of the kidney motion on the stent fatigue resistance for the single stent configuration.[16] Results showed that the stented portion of the renal arteries was relatively straight (indicating minor bending), but the renal branch angle was greater in the nonstented portion of the renal arteries. FEA revealed excellent fatigue resistance of the studied cobalt-chromium stent under simulated respiratory motion. In this article, the study was extended further to the overlapped stent configuration, where a physician has to deploy two stents overlapping at the stent ends to fully cover a long lesion. The following strategy was employed to study the overlapped stent configuration:

1. Fluoroscopic images of the stented renal arteries were taken from cadavers at simulated inspiration and expiration positions. Respiratory motion was simulated by manual manipulation of the kidneys to reflect their craniocaudal movement observed clinically.
2. Stent bending during simulated respiration was measured from fluoroscopic images and used as input parameters for the subsequent finite element model.
3. FEA was developed and performed to assess the cobalt-chromium stent bending fatigue performance during respiration.

CADAVER STUDY

A newly developed L-605 cobalt-chromium stent was used in this study. The use of this material enables a reduction in stent wall thickness relative to traditional stainless steel to improve the stent hemodynamic proper-

TABLE I. Mechanical Properties of L-605 Co-Cr Alloy

Young's Modulus (GPa)	Yield Stress (MPa)	Ultimate Stress (MPa)	Endurance Limit (MPa)	Poisson's Ratio
203	590	1689	483	0.3

ties, while retaining adequate visibility under fluoroscopy. Its family covers the nominal stent inner diameters from 4 to 7 mm. In clinical use, the stent may be postexpanded to 1 mm greater than the nominal diameter if necessary. The stents were processed by laser cutting the intended design pattern onto the surface of the hypotube, the starting tube for the manufacture of intravascular stents and other biomedical devices. The as-cut stent surfaces were then electrochemically polished to achieve a good surface finish. Mechanical properties of the L-605 cobalt-chromium alloy are listed in Table I.

To test this cobalt-chromium stent not yet approved for clinical use at the time of this work, a cadaver study was performed where two cadavers (henceforth designated as Cadaver A, Cadaver B) were used, with one male and one female at the age of ~60s. Their cause of death had no specific evidence of cardiovascular diseases or other vascular-related diseases. The cadavers were prepared based on the methods described in Ref. [17] to allow warm (body temperature) saline through the vasculature to simulate blood flow and maintain lumen pressure. The artery lumen was pressurized with saline during renal artery catheterization and stent deployment. Each cadaver was placed in the supine position. To implant stents, endovascular access to the renal arteries was obtained via the femoral artery. The first 7 × 18 mm cobalt-chromium stent was deployed into the renal arteries of two cadavers through a transfemoral approach such that the end of the stent completely covered the renal ostium where the lesion is usually located. The stent was expanded to 7 mm (inner diameter) and then postexpanded slightly. After implanting the first cobalt-chromium stent, a second stent was deployed into the renal arteries of two cadavers such

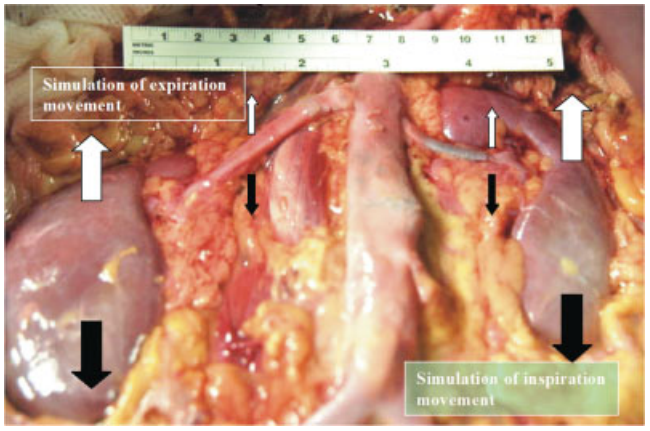

Figure 2. Simulation of the kidney and stented renal artery motion during respiration cycle. [Color figure can be viewed in the online issue which is available at www.interscience.wiley.com.]

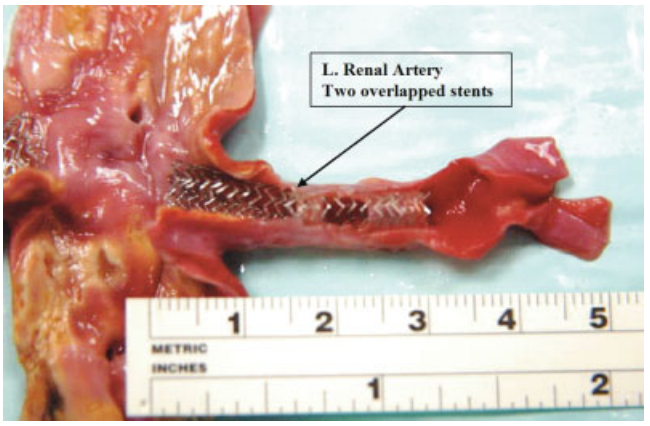

Figure 3. Explanted aortic segment with renal artery showing implanted overlapped stents. [Color figure can be viewed in the online issue which is available at www.interscience.wiley.com.]

that the proximal portion of this second stent overlapped the distal portion of the first stent by ~3–4 mm. This was to simulate the clinical situation, where a physician has to deploy two stents overlapping at the ends to fully cover a long lesion.

Surgical access to the abdominal cavity and retroperitoneal space was then obtained via midline incision through the abdominal wall. Contents of the abdominal cavity were partially removed to allow access to the renal arteries and kidneys. Mineral oil was used to lubricate the tissues of the body cavities and inside the renal arteries to ensure ease of movement of tissues against each other. Sutures were sewn to the tissues surrounding the renal arteries and umbilical tape was looped around the renal arteries at the midpoint to facilitate manual manipulation and displacement of the kidneys. It should be noted that, although saline was continuously pumped into the vasculature during procedure, lumen pressure dropped considerably due to arterial branch bleeding after surgical exposure of the kidneys and renal arteries. Respiratory movement was simulated by manual manipulation of the kidneys (Figure 2). The displacement of the kidneys was estimated to be 40 mm based on the clinical human data. The stents were implanted in the neutral position at rest. The displacements of +20 mm cranial (toward head for expiration simulation) and −20 mm caudal (toward legs for inspiration simulation) from the kidney were measured with a ruler to establish the upper and lower bounds of the kidney movement. The manual simulation of the kidney movement was attempted in such a way that the kidney movement plane was considered close to perpendicular to the plane of view. Therefore, it is believed that the measurements were able to capture the true bending angle changes. The guide wire tip position, C-Arm floor position, and cadaver position remained unchanged throughout each cycle of one simulated inspiration and expiration movement to ensure a consistent reference point. Fluoroscopic images were collected for later analysis. Figure 3 shows the explanted and opened aortic segment with two overlapped stents implanted in a renal artery.

FINITE ELEMENT ANALYSIS

Stents placed in the vasculature are subjected to various modes of cyclic loading that may consequently compromise the structural integrity of the stents during their functional life resulting in fatigue failure. In this study, FEA was performed to evaluate the stent structural integrity and fatigue resistance. Simulation was performed to ensure whether the stent will survive 4×10^8 cycles under simulated physiological environment with a combination of cardiac pulsatile fatigue loading and respiratory bending fatigue loading. Ten years of fatigue life, accepted as a standard for stents today, is equivalent to 4×10^8 cardiac systolic/diastolic cycles and $\sim 0.5 \times 10^8$–1×10^8 respiratory cycles (assuming human breath rate is 10–20 times per minute). Therefore, the combined pulsatile and bending fatigue simulation (4×10^8 cycles for each) performed in this study represents a far more conservative assessment to the studied stent fatigue resistance. The fatigue mean stress of 1689 MPa was obtained in-house using the Instron mechanical testing machine in accordance with the procedures outlined in ASTM E8-98, ASTM E83-96, and ASTM E345-93. The test procedure involved standard tensile strength testing of the L-605 cobalt-chromium tubing using extensometers for strain measurements. The fatigue alternating stress of 483 MPa was obtained from the material supplier and verified by literature publication.[18]

A finite element model was developed to evaluate the stent response to various loading conditions involved in preparing and deploying an intravascular stent consistent with clinical practice such as manufacturing (crimped onto a balloon catheter), *in vivo* deployment (expanded into an artery), and clinical vascular environment (systolic/diastolic pressure, respiration-induced bending). The stent fatigue analysis determined the state of stress and strain due to loading imposed by the following procedure:

Step 1. Stent crimping from 2.54 mm to 1.36 mm OD.
Step 2. Stent recoil after crimping.
Step 3. Stent expansion to 7.0 mm ID in an artery model.
Step 4. Stent recoil after expansion.
Step 5. Stent bending during inspiration superimposed with systolic/diastolic pressure (180/80 mmHg).
Step 6. Stent bending during expiration superimposed with systolic/diastolic pressure (180/80 mmHg).

To evaluate the stent long-term fatigue performance under the loading conditions imposed by inspiration and expiration along with the systolic and diastolic arterial blood pressure loading, a Goodman fatigue analysis was performed using the multiaxial stress state experienced in Steps 5 and 6. Since the stent is diametrically over-expanded relative to the vessel, there is a significant compressive preload imposed on the stent that results in fatigue cycling with a mean stress not equal to zero. It should be noted that mean stress could also be a result of the plastic deformations of crimping and deployment. The Goodman relation states that fatigue failure will occur if the stress state in the component satisfies the relation:

$$\left(\frac{\sigma_a}{\sigma_e}\right) + \left(\frac{\sigma_m}{\sigma_u}\right) \geq 1$$

where σ_a is the stress amplitude applied to the component, σ_e is the modified material endurance limit for non-zero mean stress, σ_m is the mean stress applied to the component, and σ_u is the material ultimate stress. The Goodman fatigue analysis was performed using the following effective mean stress and effective stress amplitude equations[19]:

$$\sigma_m = \frac{1}{\sqrt{2}}\sqrt{(\sigma_{1m} - \sigma_{2m})^2 + (\sigma_{2m} - \sigma_{3m})^2 + (\sigma_{3m} - \sigma_{1m})^2}$$

$$\sigma_a = \frac{1}{\sqrt{2}}\sqrt{(\sigma_{1a} - \sigma_{2a})^2 + (\sigma_{2a} - \sigma_{3a})^2 + (\sigma_{3a} - \sigma_{1a})^2}$$

where σ_m is the effective mean stress, σ_a is the effective stress amplitude, σ_{1m}, σ_{2m}, σ_{3m} are the principal mean stresses, and σ_{1a}, σ_{2a}, σ_{3a} are the principal stress amplitudes experienced. The principal stresses σ_1, σ_2, σ_3 were first extracted at each integration point for the combined pulsatile and bending loading conditions. These principal stresses were used to calculate the principal mean stresses and stress amplitudes. Once the principal mean stresses and stress amplitudes were determined, the effective mean stress and stress amplitude were then calculated at each integration point using the above equations.

The Goodman diagram is a plot of the normalized stress amplitude σ_a/σ_e (on the y-axis) versus the normalized mean stress σ_m/σ_u (on the x-axis). The equation $(\sigma_a/\sigma_e) + (\sigma_m/\sigma_u) = 1$ represents the failure line on the Goodman diagram for non-zero mean stress with the modified endurance limit defined as:

$$\sigma_e = \sigma_{e0}\left(1 - \frac{\sigma_m}{\sigma_u}\right)$$

where σ_{e0} is the material endurance limit for zero mean stress.

The Fatigue Safety Factor is defined as the ratio of the stress amplitude against the modified endurance limit, where the stress amplitude is the stress difference and the mean stress is the average stress on the element stresses. It quantifies the proximity of the mean stress and stress amplitude at any given numerical integration point to the limiting Goodman curve. The integration points were used instead of nodal points in this study for accuracy and consistency reasons. Although the integration points do not allow for recovered surface stresses, they offer the true

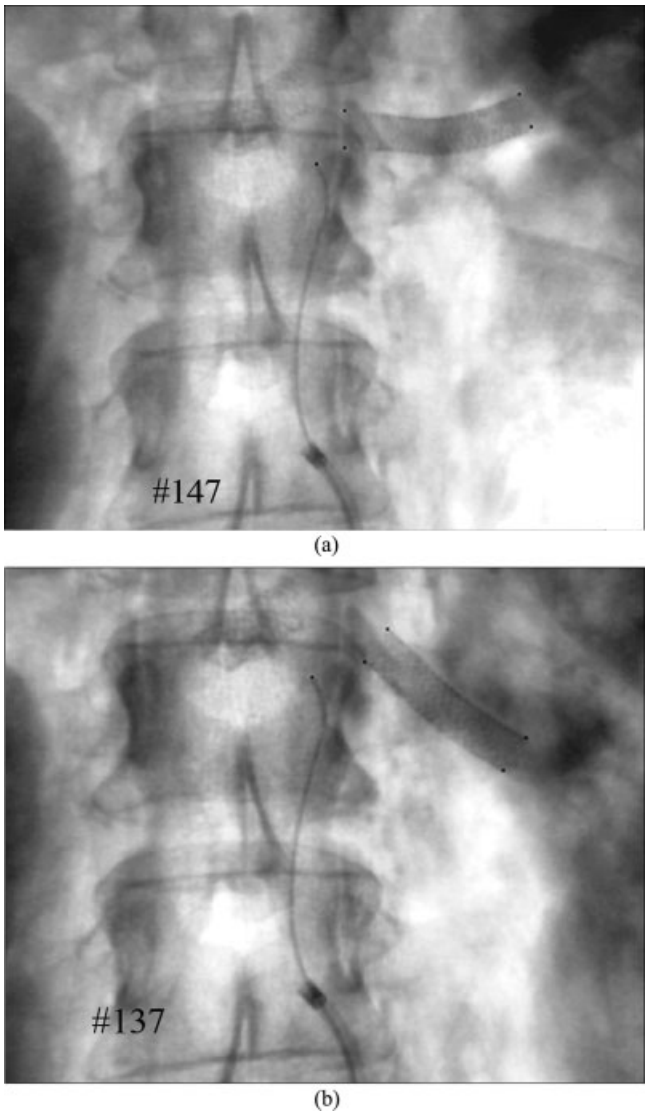

Figure 4. Fluoroscopic images of stented renal arteries at simulated respiration positions (a) Expiration, (b) Inspiration.

exact solution without any extrapolation errors associated with nodal values. Fatigue Safety Factor less than 1.0 indicates a fatigue failure.

$$\mathrm{FSF} = \frac{\sigma_e}{\sigma_a}$$

RESULTS

Respiration-Induced Stent Bending Angle Measurement

Figure 4 shows the representative fluoroscopic images of stented renal arteries at simulated inspiration and expiration positions for the overlapped stents. As shown, the stents were subjected to bending during respiration with significant rigid body motion (translation and rotation) involved. Rigid body motion does not contribute to the stent deformation and was therefore ignored in the analysis. It is interesting to note that, for the single stent configuration previously studied,[16] the stented portion of the renal arteries was relatively straight (indicating minor bending), thus pushing the vessel bending distally toward the kidney during expiration. Whether or not the vessel kinked just beyond the end of the stent could not be determined due to lack of sufficient pressurization during respiratory simulation. However, for the overlapped stent configuration in this study, the overlapped stents took the bending curvature of the renal arteries smoothly, but they were apparently subjected to greater degree of bending.

Kidney motion during respiration results in bending of the renal arteries, thereby deforming the longitudinal axis of the stent into a curved line. Figure 5(a) illustrates the deflection curve of a stent subjected to bending. A line tangent to the deflection curve at the stent end forms angle θ to the x-axis that represents the bending angle of the stent. When drawing tangent lines to the deflection curve from both ends, based on analytic geometry, the acute intersection angle of these two tangents is 2θ that is twice the defined bending angle.

When the bending curvature is nonuniform along the stent length, the bending angle is defined as θ for one end and ϕ for the other end. As a result, the intersection angle of the two tangents is $\theta + \phi$ instead of 2θ. Procedures to determine the bending angle at the stent ends were:

1. Imported fluoroscopic images to AutoCAD software (AutoCAD LT 2000i).
2. Ignored rigid body motion (both translation and rotation).
3. Drew tangential lines to the deflection curve at the stent ends.
4. Measured the acute intersection angle $\theta + \phi$ of the two tangents.

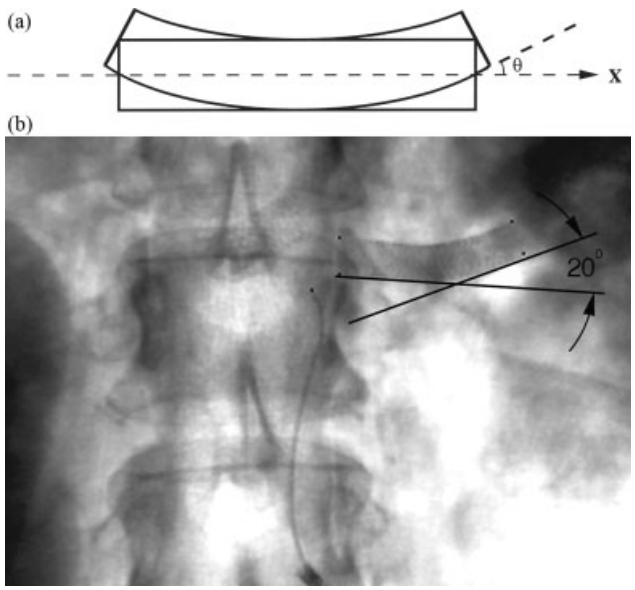

Figure 5. (a) Deformations of a stent in bending, (b) Measured acute intersection angle at expiration.

5. Divided $\theta + \phi$ by 2. This is the average bending angle at the end points of the stent. The average bending angle can be related to the average curvature κ or average radius of curvature ρ with the following definition:

$$\kappa = 1/\rho = 2(\text{average bending angle})/L = (\theta + \phi)/L$$

where L is the combined stent length.

The example shown in Figure 5(b) has the measured acute intersection angle of 20°. In this case, the resulting average bending angle at the stent end is half of that value, 10°, and its corresponding curvature is 0.011 mm^{-1} (radius of curvature: 92 mm). It is interesting to note that, since the intersection point of the two tangents is not at the stent mid point, this implies that the stent bending deformation is not uniform.

Table II summarizes the average measured bending angle at the stent ends from fluoroscopic images and the average calculated bending curvature for the overlapped stent configuration. As shown, the bending angle changed from 2.75° to 11.75° on an average basis. The change in bending angle between inspiration and expiration was ~9°, which is considerably greater than the single stent configuration previously reported. The increased bending angle measured at the stent ends of the overlapped stents was partially due to larger bending curvature and partially due to longer overall stent length.

This information was used for the subsequent FEA wherein these bending angles/curvatures were superimposed upon forces associated with high hemodynamic pressure (blood pressure 180/80 mmHg) to simulate conditions achievable in the intended patient population.

Stent Fatigue Resistance

Stents deployed in the overlapped configuration were studied. Two 18-mm long stents, the standard implant size for renal stenting, were overlapped at the stent ends by 3–4 mm, making the total stented renal artery length of ~32–33 mm. This was to simulate the less-occurred clinical situation in renal applications, where a physician has to deploy two stents overlapping at the ends to fully cover a long lesion. Although uncommon in renal stenting, this is a very common clinical practice in other applications such as coronary stenting.

The ABAQUS/Standard finite element solver was used to perform the stent fatigue analysis. To prevent shear locking induced by bending loads, the stent struts were modeled using C3D8I fully integrated 3D solid elements with incompatible modes. The models were three-layers deep through the thickness and contained six elements in the width dimension to ensure that stress variation was adequately captured. Mesh density studies of similar problems were performed to select the appropriate mesh density for the representative stress and strain distribution throughout the stent. It was concluded from the studies that the maximum stresses with the selected 6 × 3 mesh were able to converge within 5% of the true values.

The mid-section of the stent was free to deform during crimping and expansion. Contact surfaces were defined at the strut edges to prevent interpenetration between the struts during the crimping process. Additional contact surfaces were imposed as needed on the outer and inner stent surfaces to provide stent interaction with the crimping and expanding rigid surfaces during the crimping and expansion processes. The analytical rigid surfaces were defined to change in radius with each increment during the simulation. Contact was removed between the stent and rigid surface during the recoil phases to allow the stent-free deformation. The recoil process resulted in the relaxation of elastic strain energy and did not incur any change in the plastic strain distribution. A blood pressure of 180 mmHg systole and 80 mmHg diastole was used during steps 5–6 to simulate the cyclic fatigue loading applied to the stent. To account for the loading imposed by the arterial wall, an arterial pressure loading corresponding to the interaction between the stent and the artery was imposed on the stent.[20,21] The bending fatigue model consisted of four stent rings, ~1/3 of the single stent length. When two stents are deployed in a tortuous vessel and overlapped, the overlapped section is relatively stiff compared to the other two free ends. Therefore, the overlapped section of the stent was considered to be the fixed end with the nonoverlapped section of the stent hanging free. The analytical rigid surface was defined to change in bending curvature during the simulation. The applied bending curvatures to the FEA model were calculated based on the average bending angles measured from fluoroscopic images of the cadaver study.

Figures 6–8 show the contour plots of von Mises stress developed during the different steps of the loading process (crimping, expansion, and bending coupled with pulsatile pressure loading) for the studied cobalt-chromium stent. The maximum von Mises stresses and maximum equivalent plastic strains at each loading step occurred on the inner

TABLE II. Bending Angle and Curvature (Overlapped Stent Configuration)

Cadaver	Inhale Bending Angle, $(\theta + \phi)/2$	Exhale Bending Angle, $(\theta + \phi)/2$	Inhale Bending Curvature (mm^{-1})	Exhale Bending Curvature (mm^{-1})
A	0°	11.0°	0	0.012
B	5.5°	12.5°	0.006	0.014
Average	2.75°	11.75°	0.003	0.013

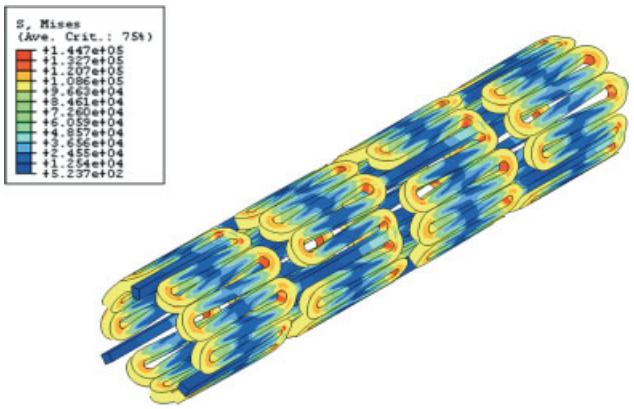

Figure 6. Contours of von Mises stress for studied cobalt-chromium stent at crimping. [Color figure can be viewed in the online issue which is available at www.interscience.wiley.com.]

surface of the curved crown "U," "Y," and "W" struts of the model. A Goodman diagram of bending fatigue coupled with pulsatile fatigue is shown in Figure 9(b) for the overlapped stent configuration. Calculated data were below the Goodman diagram failure line, indicating that the studied cobalt-chromium stents in the overlapped configuration are able to pass the fatigue life of 4×10^8 cycles under combined pulsatile and bending fatigue.

DISCUSSION

Stents deployed in the overlapped configuration were studied. This was to simulate the clinical situation in renal applications where a physician has to deploy two stents overlapping at the ends to fully cover a long lesion. The overlapped stents implanted in renal arteries behave in a different way during simulated respiration-induced kidney motion when compared to a single stent. For the single stent configuration, the stented portion of the renal arteries was relatively short and straight, pushing most of the vessel tortuosity distally toward the kidney. As a result, the stent

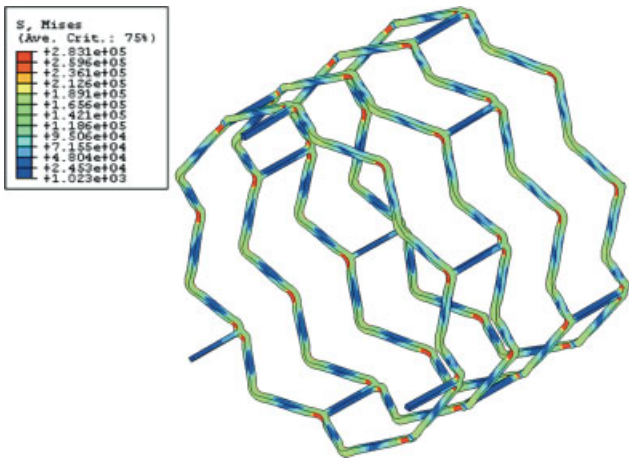

Figure 7. Contours of von Mises stress for studied cobalt-chromium stent at expansion. [Color figure can be viewed in the online issue which is available at www.interscience.wiley.com.]

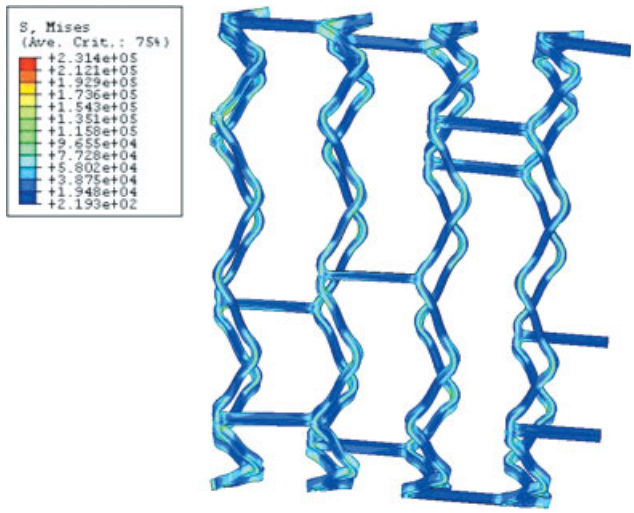

Figure 8. Contours of von Mises stress for studied cobalt-chromium stent under bending coupled with pulsatile pressure loading. [Color figure can be viewed in the online issue which is available at www.interscience.wiley.com.]

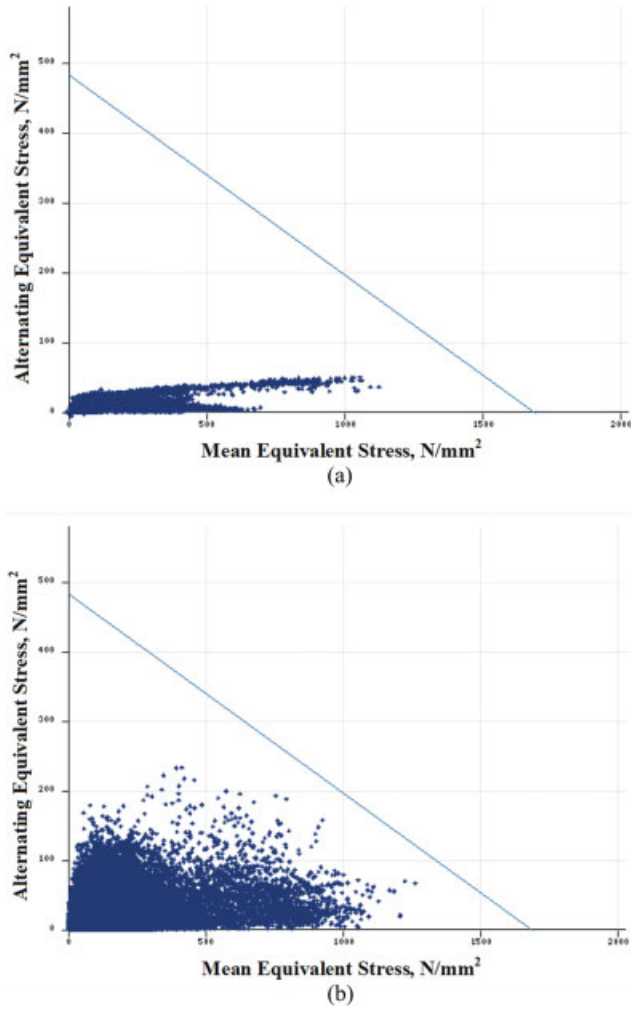

Figure 9. Goodman diagram for studied cobalt-chromium stent (a) Pulsatile fatigue, (b) Combined pulsatile and bending fatigue. [Color figure can be viewed in the online issue which is available at www.interscience.wiley.com.]

was only subjected to minor bending and affected less by kidney motion. However, for the overlapped stent configuration, the longer overlapped stents were forced to conform to the bending curvature of the renal arteries and apparently subjected to greater degree of bending than the single stent. Comparing Figure 9(b) to 9(a) where the very same stent was assessed for pulsatile fatigue alone, it is shown that the calculated data of the overlapped stents under combined pulsatile and bending fatigue migrated toward the Goodman diagram failure line, indicating a drop in Fatigue Safety Factor and thus lower fatigue resistance during respiration. This finding also implies that, should longer stents be used clinically in renal applications, more pronounced respiration-induced bending may occur on stents. The degree of bending is likely to increase as the overall stent length becomes longer. The stented portion of the renal artery would become long enough such that it is forced to conform to the curvature the renal artery forms during respiration. Therefore, it is likely that a longer stent or multiple overlapped stents would have a shorter fatigue life than a shorter stent in renal applications. Since most of the renal artery stenosis occurs at the renal ostial region (renal artery and aorta junction), this short region should become the primary focus of the treatment instead of stenting long section of the renal artery that requires a long stent or multiple overlapped stents.

It should be noted that the simulated distance between inspiration and expiration (about 40 mm) used in this study represents greater degrees of bending than the actual bending normally seen in the overlapped stent case. The reason for this is that when two stents are overlapped, the entire renal artery becomes stiff enough such that, under similar respiratory forces, the kidney movement may be constrained and thus the movement is not as pronounced as 40 mm observed in other studies during normal breathing with no stents implanted. Therefore, it is hypothesized that the overlapped stent results presented in this article were considered as the worst case scenario that may be more conservative than the actual.

The stent design also plays a very critical role in the stent bending fatigue resistance. When the stent design is less flexible (in contrast to the studied cobalt-chromium stent which is very flexible), it tends to straighten out the vessels considerably and pushes the vessel tortuosity distally. This could create kink points at the stent/vessel junctions, which could disturb the blood flow and trigger adverse events such as vessel spasm and thrombosis. Such stiffer stent is also likely to have a shorter fatigue life due to the higher stresses created by the stent design itself and its interaction with the surrounding vessel movement. Therefore, it is very important to select the appropriate stent designs for specific applications. For applications subjected to greater degrees of bending such as renal artery and superficial femoral artery, a flexible stent design is preferred and should be used. However, for other applications such as carotid stenting where the primary concern is the potential stroke risk of emboli dislodgement from plaque, a stent with greater scaffolding should be considered as the main candidate to help pave the artery better.

CONCLUSION

The purpose of this study was to determine whether the motion of the kidneys during respiration, and subsequent bending of the renal artery, would negatively impact stent bending fatigue performance when two stents are overlapped. To address this issue, stents were deployed into renal arteries of two cadavers and respiratory motion was simulated by manual manipulation of the kidneys. Stent bending angles were measured from fluoroscopic images and FEA was performed.

The change in bending angle, after compensation for rigid body motion, was more significant for the overlapped stent configuration. Measured bending angles/curvatures applied to FEA indicated that the fatigue resistance became lower as a result of greater degrees of bending, when compared to the single stent configuration from previous study. Results showed that the studied cobalt-chromium stent is not at risk for bending fatigue failure during respiratory motion for both single and overlapped stent configurations.

The authors gratefully acknowledge Danielle LaFlash, Kelly Pike, and Dr. Henjen Ho for their help. The continued support of the program by the following individuals is acknowledged with sincere appreciation: Dr. Richard Rapoza, Dr. John Boylan, Keif Fitzgerald, and Robin Eckert.

REFERENCES

1. Blum U, Krumme B, Flugel P, Gabelmann A, Lehnert T, Buitrago-Tellez C, Schollmeyer P, Langer M. Treatment of ostial renal-artery stenoses with vascular endoprostheses after unsuccessful balloon angioplasty. N Engl J Med 1997;336: 459–465.
2. Zeller T, Frank U, Muller C, Burgelin K, Sinn L, Bestehorn H, Cook-Bruns N, Neumann F. Predictors of improved renal function after percutaneous stent-supported angioplasty of severe atherosclerotic ostial renal artery stenosis. Circulation 2003;108:2244–2249.
3. Rocha-Singh K, Jaff MR, Rosenfield K. Evaluation of the safety and effectiveness of renal artery stenting after unsuccessful balloon angioplasty. J Am Coll Cardiol 2005;46:776–783.
4. Bessias N, Sfyroeras G, Moulakakis KG. Renal artery thrombosis caused by stent fracture in a single kidney patient. J Endovasc Ther 2005;12:516–520.
5. Sahin S, Memis A, Parildar M, Oran I. Fracture of a renal artery stent due to mobile kidney. Cardiovasc Intervent Radiol 2005;28:683–685.
6. Moerland MA, van den Bergh AC, Bhagwandien R, Janssen WM, Bakker CJ, Lagendijk JJ, Battermann JJ. The influence of respiration induced motion of the kidneys on the accuracy of radiotherapy treatment planning, a magnetic resonance imaging study. Radiother Oncol 1994;30:150–154.

7. Schwartz LH, Richaud J, Buffat L, Touboul E, Schlienger M. Kidney mobility during respiration. Radiother Oncol 1994;32:84–86.
8. Davies SC, Hill AL, Holmes RB, Halliwell M, Jackson PC. Ultrasound quantitation of respiratory organ motion in the upper abdomen. Br J Radiol 1994;67:1096–1102.
9. Ahmad NR, Huq MS, Corn BW. Respiration-induced motion of the kidneys in whole abdominal radiotherapy: Implications for treatment planning and late toxicity. Radiother Oncol 1997;42:87–90.
10. Draney M, Zarins CK, Taylor CA. Three-dimensional analysis of renal artery bending motion during respiration. J Endovasc Ther 2005;12:380–386.
11. Harrison WJ, Lin ZC. The study of nitinol bending fatigue. In: Proceedings of the International Conference on Shape Memory and Superelastic Technologies, Pacific Grove, CA, SMST Society, Inc. 2000. pp 391–396.
12. Pelton AR, Gong XY, Duerig TW. Fatigue testing of diamond-shaped specimens. In: Proceedings of the International Conference on Shape Memory and Superelastic Technologies. Menlo Park, CA: SMST Society, Inc.; 2003. pp 293–302.
13. Wagner M, Sawaguchi T, Kaustrater G, Hoffken D, Eggler G. Structural fatigue of pseudoelastic NiTi shape memory wires. Mater Sci Eng A 2004;378:105–109.
14. Marrey RV, Burgermeister R, Grishaber RB, Ritchie RO. Fatigue and life prediction for cobalt-chromium stents: A fracture mechanics analysis. Biomaterials 2006;27:1988–2000.
15. Robertson SW, Ritchie RO. In vitro fatigue-crack growth and fracture toughness behavior of thin-walled superelastic nitinol tube for endovascular stents: A basis for defining the effect of crack-like defects. Biomaterials 2007;28:700–709.
16. Hsiao HM, Prabhu S, Nikanorov A, Razavi M. Renal artery stent bending fatigue analysis. J Med Devices 2007;1:113–118.
17. Garrett HE, Jr. A human cadaveric circulation model. J Vasc Surg 2001;33:1128–1130.
18. Bjork VO, Lindblom D, Henze A. The monostrut strength. Scand J Thorac Cardiovasc Surg 1985;19:13–19.
19. Suresh S. Fatigue of Materials. Cambridge, UK: Cambridge University Press; 1991.
20. Gizdulich P, Wesseling KH. Forearm arterial pressure-volume relationships in man. Clin Phys Physiol Meas 1988;9:123–132.
21. Muntinga JHJ, van Leeuwen JTM, Gels ME, Terpstra WF, Smit AJ, Visser KR. Arteriolar constriction in mild-to-moderate essential hypertension: An old concept requiring reconsideration? J Hypertens 1997;15:411–419.